frontiers | Frontiers in Materials

ORIGINAL RESEARCH
published: 28 April 2022
doi: 10.3389/fmats.2022.899112

Shear Mechanism of High-Strength-Friction-Grip Bolts in Steel and Steel-Fiber-Reinforced-Concrete Composite Beams

Yujie Zhang[1], *Junping Zhang*[2]*, *Bingcong Chen*[3]* *and Yumin Zhang*[4]

[1]College of Urban and Rural Construction, Zhongkai University of Agriculture and Engineering, Guangzhou, China, [2]Earthquake Engineering Research and Test Center, Guangzhou University, Guangzhou, China, [3]Research Center for Wind Engineering and Engineering Vibration, Guangzhou University, Guangzhou, China, [4]College of Urban Construction, Heze University, Heze, China

Steel and steel-fiber-reinforced concrete (SFRC) composite beams with high-strength friction-grip bolt (HSFGB) connectors have been found to improve the shear behavior of HSFGBs and enhance the potential application of composite beams. In order to evaluate the shear force transmission mechanism of HSFGBs in steel-SFRC beams, finite element models (FEMs) developed by ABAQUS software had been carefully developed to evaluate force transmission and failure mechanisms of HSFGBs. Shear behavior differences between conventional studs and HSFGBs were also studied. Then according to the orthogonal statistics method, FEMs were further modified to explore significant influencing factors affecting HSFGB shear performance. The results showed that pretension degree was the main factor affecting the shear performance of HSFGBs at serviceability limit states, while HSFGB diameter was the most important factor affecting stiffness and ultimate shear strength at ultimate limit state.

Keywords: high-strength friction-grip bolt, steel-fiber-reinforced concrete, shear performance, transmission mechanism, composite beams

OPEN ACCESS

Edited by:
Tianyu Xie,
RMIT University, Australia

Reviewed by:
Shan Gao,
Harbin Institute of Technology, China
Zhuangcheng Fang,
Guangdong University of Technology, China

***Correspondence:**
Junping Zhang
zhang-jp@139.com
Bingcong Chen
bc_chen@gzhu.edu.cn

Specialty section:
This article was submitted to Structural Materials, a section of the journal Frontiers in Materials

Received: *18 March 2022*
Accepted: *01 April 2022*
Published: *28 April 2022*

Citation:
Zhang Y, Zhang J, Chen B and Zhang Y (2022) Shear Mechanism of High-Strength-Friction-Grip Bolts in Steel and Steel-Fiber-Reinforced-Concrete Composite Beams. Front. Mater. 9:899112. doi: 10.3389/fmats.2022.899112

1 INTRODUCTION

Due to their outstanding properties such as favorable mechanical characteristics, easy construction, and beneficial economic performance, steel-concrete composite beams have been extensively applied in engineering for many years (Brozzetti, 2000; Nakamura et al., 2002). As an important component of composite beams, shear connectors directly affect the overall performance of composite beams. Generally, stud connectors are applied to transmit joint action between the steel beam and concrete slabs (Oehlers and Bradford, 1995). However, conventional headed stud connectors welded onto steel beams and cast into concrete slabs limit the repairability of composite beams. Furthermore, shrinkage and creep of cast-in-place concrete slabs connected by headed studs might result in the increase of composite beam deformation, greatly affecting the long-term performance of composite structures (Johnson, 2006; Ban et al., 2015).

One way to address these issues is the application of HSFGBs as shear connectors in composite beams due to their advantages of high strength and stiffness, tight connection, and convenience of dismantling. However, due to the lower load at initial slip and cracking of concrete slabs (Zhang et al.,

2019), HSFGB properties may not be fully developed. Meanwhile, steel-fiber-reinforced concrete (SFRC) specimens fabricated by the addition of steel fibers into normal concrete have superior tensile strength and favorable ductility (Khaloo and Afshari, 2005; Taniguchi et al., 2007), can effectively control crack development. Also, the application of SFRC in the negative bending moment region of continuous composite beams not only effectively restrained the crack width in slabs but also improved the ultimate capacity of composite beams (Lius et al., 2006; Abas et al., 2013; Lin et al., 2016). Therefore, the application of SFRC with high tensile strength and crack resistance in composite beams was found to improve the shear behavior of HSFGBs and enhance the potential application of composite beams. Due to the abovementioned advantages, these innovative composite beams with HSFGBs can be extended to the rapid construction of small and medium span bridges, as well as steel-concrete composite flooring systems.

Dallam (1968) and Harpster (Dallam and Harpster, 1968) performed static push-out tests on steel-concrete composite specimens connected by the HSFGBs. The test results revealed that the ultimate load of HSFGB connectors was higher than that of studs. Dedic and Klaiber (1986) studied the behaviors of HSFGBs to reinforce existing non-composite bridges. The obtained test results showed that HSFGBs could increase the strength of non-composite bridges. Pavlović et al. (2013) performed experimental tests and numerical analyses on HSFGBs and found that although they had sufficient shear strength, their shear stiffness was lower than that of headed studs. Kwon et al. (2010; 2011) evaluated the application of HSFGBs with embedded nuts in prefabricated concrete slabs and found that HSFGBs had a lower shear capacity and initial stiffness than headed studs. [Liu et al., (2015); Liu and Bradford, (2016)] performed a series of research works on the shear behavior of HSFGBs. However, they noted undesirable large slips, which negatively affected the shear stiffness of bolts. Zhang et al. (2019) studied the shear behavior of HSFGBs and found that the shear capacity and stiffness of bolted connectors were reduced due to the cracks in concrete slabs. Recently, Ataeiet et al. (2019) reported that increasing the size and strength of single-nut bolts enhanced initial stiffness, ultimate shear strength, ductility, and energy dissipation capacity. Furthermore, HSFGBs have been applied for connecting the steel beams and precast ultra-high-performance concrete (Fang et al., 2020; Fang et al., 2021; Fang et al., 2022) and it has been found that HSFGBs improved the performance of composite beams with ultra-high-performance concrete.

Among previous research works reported in the literature, most studies have focused on the factors influencing the ultimate shear capacity of HSFGBs at the ultimate limit state (Kwon et al., 2010; Liu et al., 2015; Liu and Bradford, 2016; Fang et al., 2020; Zhang et al., 2020). However, HSFGBs are employed to connect steel beams and concrete slabs by applying pretension. In addition, the interfacial shear force is transmitted through the friction generated by HSFGB pretension at the initial loading stage which is then transmitted through extrusion between bolts and concrete slabs [GB/T 3632-2008, 2008/T 3632-2008 (2008). Na, 2008] Therefore, it was necessary to investigate the shear performance of HSFGBs at initial loading and ultimate limit stages. It is of pivotal importance to obtain the transmission regularity of shear force for the design of HSFGBs in steel-concrete composite beams. Therefore, studying deeply shear transfer mechanism of HSFGBs has important theoretical and engineering value. However, little research has been conducted on the force transmission mechanism of HSFGBs in composite beams. Therefore, effective finite element models (FEMs) were developed to investigate the load transfer and failure mechanisms as well as significant influencing factors on the shear behaviors of HSFGBs.

2 FINITE ELEMENT ANALYSIS

FE method was applied to further investigate the shear performance and force transmission mechanism of HSFGB connections in SFRC specimens. To obtain accurate numerical results, all components including concrete slabs, steel beams, bolted connectors, reinforcing bars, and washers were appropriately modeled in FE analyses. Both geometrical and material nonlinearities were taken into account.

2.1 Finite Element Modeling

2.1.1. Numerical Models

The 3D FEMs of specimens were established by using finite element analysis software ABAQUS. As shown in **Figure 1**, one-quarter of each specimen was simulated by applying symmetric constraints on a symmetric surface. In the developed FEMs, concrete slabs, bolts, washers, and structural steel beams were simulated by 3D eight-node linear hexahedral solid element (C3D8R) in ABAQUS. Reinforcing bars were modeled by 3D truss elements (T3D2). Surface-to-surface contact interaction was applied at all interfaces by setting contact pairs, as shown in **Figure 2**. Hard contact was applied for normal behavior, while tangential behavior was supposed as a penalty option. The reinforcement bars were embedded in a concrete slab, as described in **Figure 2C** (Han et al., 2015).

To prevent out-of-plane deformations, symmetric planes (surfaces 1 and 3) were set as symmetric boundary conditions, and the bottom of the concrete slab (surface 2) was completely restrained (Wang et al., 2021). Displacement loading was applied on the top of the steel beam, as shown in **Figure 3**.

2.1.2 Material Properties

2.1.2.1 Steel

The stress-strain relationship introduced by Zhang et al. (2020) was applied to represent the constitutive behaviors of HSFGBs. The stress-strain behaviors of steel plates and rebar were supposed to be elastic.

2.1.2.2 Concrete

Concrete behavior was modeled by the concrete damaged plasticity (CDP) model in ABAQUS.**Figure 4** shows equivalent

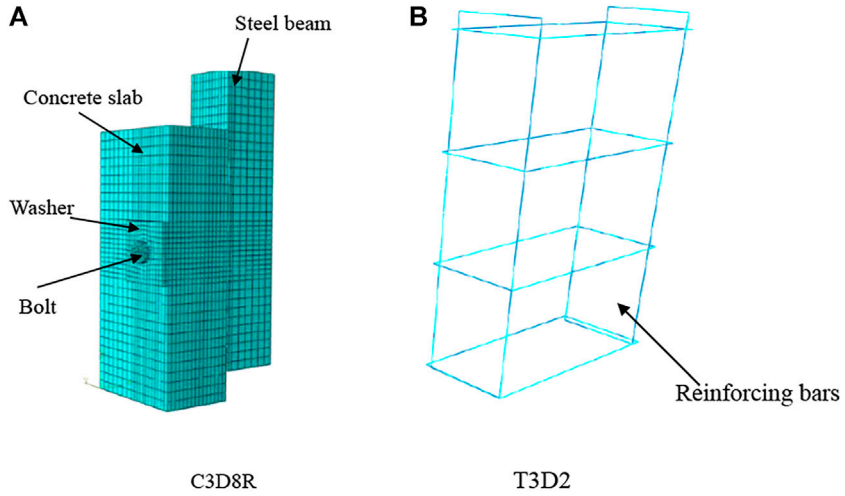

FIGURE 1 | Details of the developed FEMs.

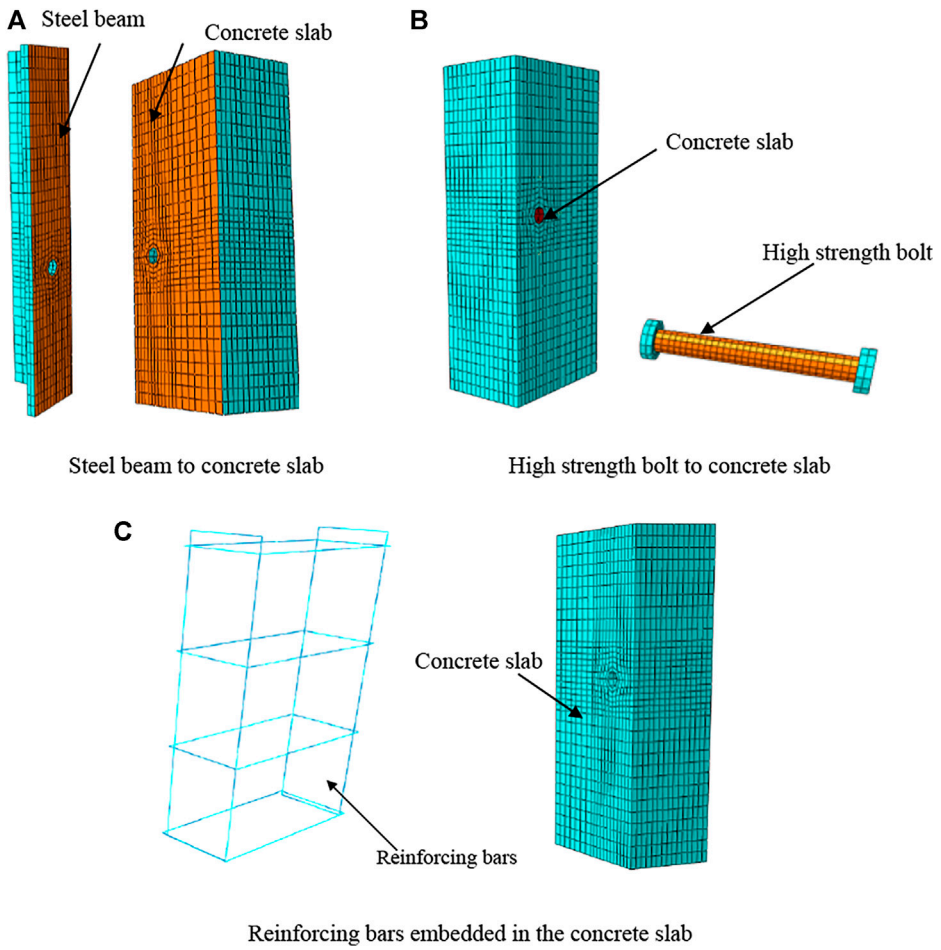

FIGURE 2 | Contact details of the developed FEMs.

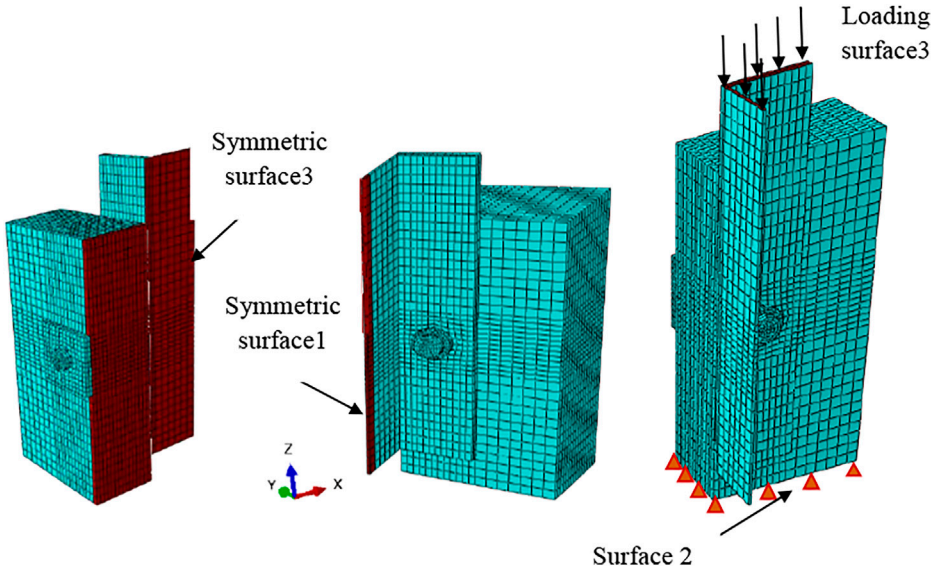

FIGURE 3 | Boundary conditions and loading surfaces.

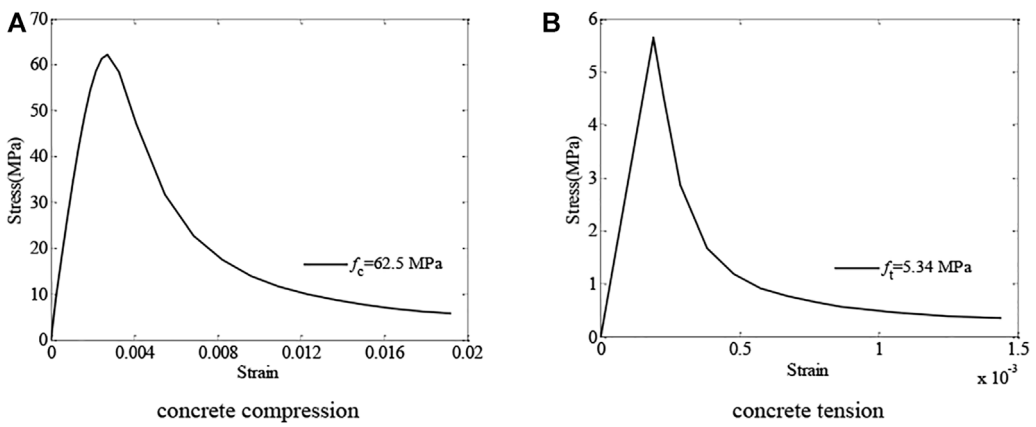

FIGURE 4 | Stress-strain curves of SFRC

uniaxial stress-strain curves, which were applied to describe the nonlinear characteristics of SFRCs.

The uniaxial stress-strain relationship suggested by Gao (1991a; 1991b) was applied to simulate SFRC behavior which was expressed as

$$\sigma_c = \begin{cases} f_c\left[ax + (3-2a)x^2 + (a-2)x^3\right] & x \le 1 \\ f_c\left[\dfrac{x}{R(x-1)^2 + x}\right] & x > 1 \end{cases}, \quad (1)$$

and

$$\sigma_t = \begin{cases} 1.2x - 0.2x^6 & x \le 1 \\ x \Big/ \left[\alpha_{ft}(x-1)^{1.7} + x\right] & x > 1, \end{cases} \quad (2)$$

where

$$x = \frac{\varepsilon}{\varepsilon_c}, \text{or } x = \frac{\varepsilon}{\varepsilon_t},$$
$$a = E_c\left(1.3 + 0.014 f_c + 0.96\gamma_f\right) \Big/ f_c \times 10^3, \quad (3)$$
$$R = \left(1.4 + 0.012 f_c^{1.45}\right)\left(1 - 0.8\gamma_f^{0.295}\right), \ \alpha_{ft} = \frac{0.312 f_t^2}{1 + 1.83\gamma_f}$$

where E_c is the elastic modulus of SFRC, f_c and f_t are uniaxial compressive and tensile strengths of concrete, respectively, ε_c is strain at compressive peak stress, ε_t is strain at tensile peak stress, and γ_f is the characteristic parameter of steel fiber concrete.

2.2 Validation of Numerical Results

In order to validate the accuracy of the finite element model developed, the push-out specimens with HSFGB tested by Zhang

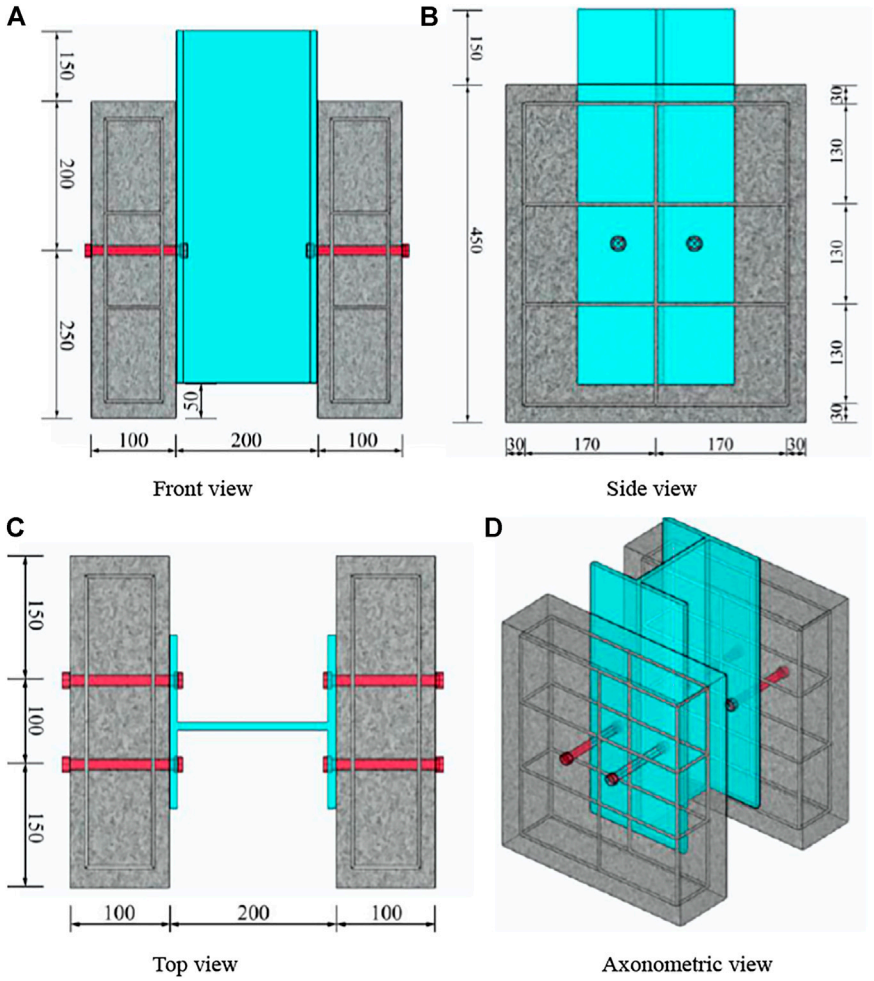

FIGURE 5 | Configurations of test specimens.

et al. (2020) have been analyzed. **Figure 5** shows specimen dimensions. The length, depth, and width of concrete slabs were 450, 120, and 440 mm, respectively (British Standards Institu, 2006). In each specimen, concrete slabs and steel beams were connected with four bolts, as presented in **Figure 5**. Bars 10 mm in diameter were applied as transverse and longitudinal reinforcements to prevent slab splitting. 500 mm long Q345 steel with a Chinese HW200 × 200×8/12 mm section was used as a steel beam.

At the initial phase of the loading process of HSFGBs, the shear force was mainly transmitted through interfacial friction. In this stage, the load-slip curve was linear which could be defined as a serviceability limit state. By the increase of load, the shear force was mainly transmitted through the force generated by the extrusion of bots and concrete slabs, where load-slip curves presented a nonlinear trend and stiffness became lower than that at serviceability limit states. This stage could be defined as an ultimate limit state. In order to systematically investigate HSFGB shear performance, the initial slip force V_0, the ultimate capacity of HSFGBs V_u, post-slipping stiffness K_s, and ultimate slipping S_u were defined as referred to reference (Zhang et al., 2020). The initial shear stiffness K_0 of HSFGBs was defined as the ratio of slip resistance load to corresponding slip value. HSFGB mechanical properties at serviceability limit state could be evaluated by initial slip force V_0 and initial shear stiffness K_0, while its mechanical properties at ultimate limit state could be evaluated by ultimate capacity V_u, ultimate slipping S_u, and post-slipping stiffness K_s.

Figure 6 a to d present the load-relative slip curves of tested specimens and the results predicted by FEM. In these figures, linear properties measured by FEM agreed well with the experimental results. However, the nonlinear response was slightly different. The reason for these differences was that the constitutive inhomogeneity of concrete was simplified in FE analyses. The accuracy range of force V_0 at initial slip between numerical and experimental results was 2.78%. Also, the accuracy range of initial shear stiffness K_0 between numerical and experimental results was 6.08%. The maximum difference between post-slipping stiffness K_s between numerical and experimental results was 9.73%, while the maximum difference between numerical and experimental values of ultimate capacity

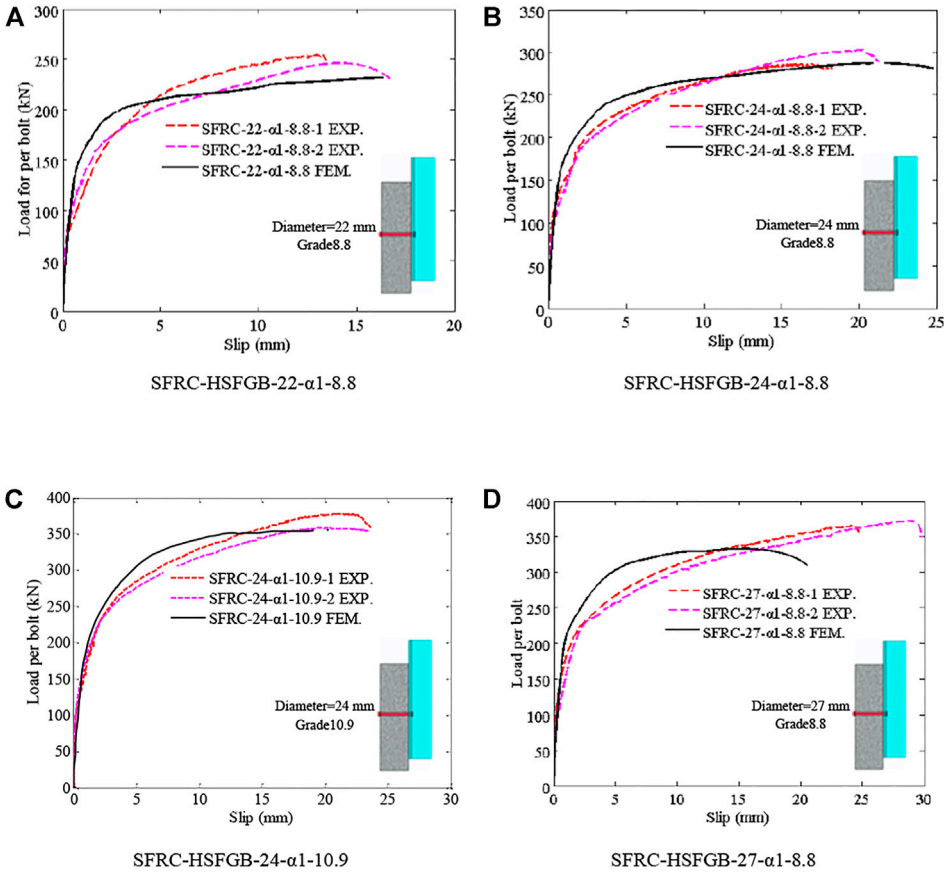

FIGURE 6 | Comparison of the numerical and tested results obtained for load-relative slip relationship.

V_U was 9.93%. Although there were some differences between numerical and experimental results, load-slip curves obtained by both methods agreed well, demonstrating that numerical models could be used for the evaluation of HSFGB shear behavior with good precision.

3 COMPARISON OF THE SHEAR PERFORMANCE OF DIFFERENT SHEAR CONNECTORS

The effect of shear connector type is shown in **Figure 7**. Two shear connector types were considered in this work: conventional headed studs and HSFGBs with a diameter of 22 mm. **Figure 6** compares load-relative slip curves of headed studs and HSFGBs. It was clearly observed that the load-relative slip curves of specimens with headed studs presented three distinct stages of linear stage (OP), nonlinear stage (PM), and descending stage (MN) while those of specimens with HSFGBs showed four distinct stages of almost no slipping stage (OA), linear stage (AB), nonlinear stage (BC), and descending stage (CD). The initial slip force in HSFGBs was more obvious than that in the headed studs due to the existence of pretension in HSFGBs. The ultimate slipping of HSFGBs was higher than that of conventional-headed studs. The ultimate capacity of headed studs and HSFGBs were 238.9 and 242.8 kN, respectively, indicating their comparable ultimate shear capacity.

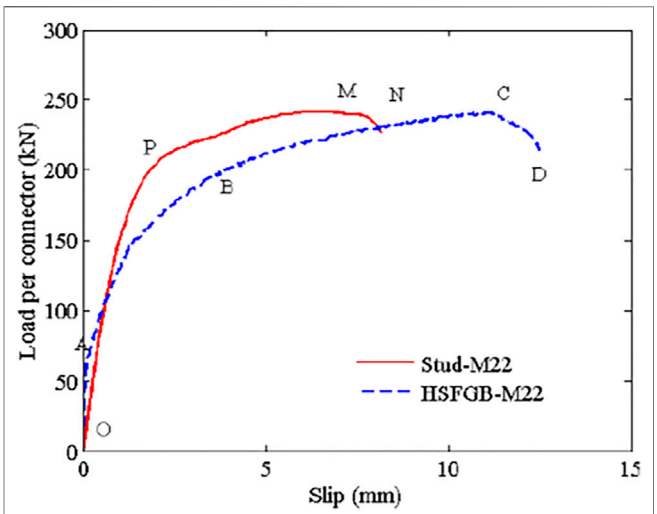

FIGURE 7 | Comparison of the shear performance of different shear connectors.

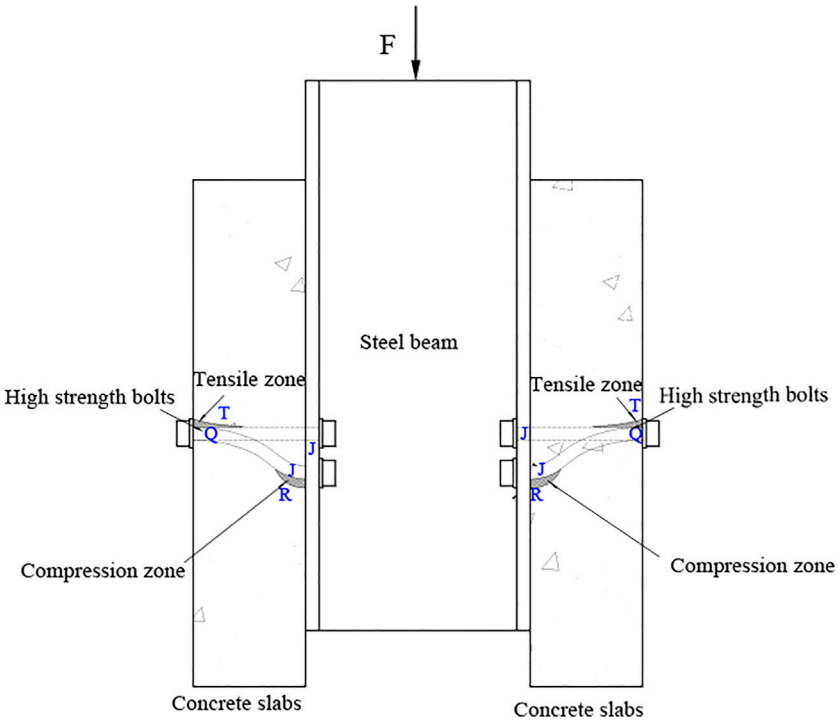

FIGURE 8 | Schematic diagram of the critical areas of HSFGBs and concrete slabs.

4 ANALYSIS OF THE FORCE TRANSMISSION MECHANISM OF HIGH STRENGTH FRICTION GRIP BOLTS

Shear failure of bolts in specimens with 22 mm grade 8.8 bolts and crushing failure of concrete slabs in specimens with 24 mm grade 10.9 bolts were observed in tests performed by Zhang et al. (2020). Hence, based on FEM results, taking specimens SFRC-HSFGB-22-α1-8.8 and SFRC-HSFGB-24-α1-10.9 as examples, internal stress distribution, as well as failure initiation and development in HSFGBs and concrete slabs in different specimens was studied and then, the force transmission mechanism, of HSFGBs was evaluated under two different failure modes.

HSFGB at the steel-concrete interface was critical during the loading process. As shown in **Figure 8**, bolts at the steel-concrete interface were marked as J and those at the end of concrete slabs were marked as Q. Meanwhile, the tensile and compression zones of concrete slabs were respectively marked as T and R.

Figure 9A shows the stress-load curves of the J zones of HSFGBs in SFRC-HSFGB-M22-α1-8.8 and SFRC-HSFGB-24-α1-10.9 specimens. **Figure 9B** presents the maximum principal stress-load curves of the T zones of concrete slabs in the abovementioned two specimens. **Figure 10** shows the typical load-slip curves of HSFGBs in the above two specimens. As shown in **Figure 9A**, the stress-load curves of the J zones of HSFGBs experienced four distinct stages: friction transferring force stage, bolt shank elastic transferring force stage, bolt shank plastic transferring force stage, and failure stage. In the friction transferring force stage (OA segments), tensile stress in the J zones of HSFGBs remained unchanged and external load was balanced by the friction force due to the pretension applied in bolts. When maximum friction force was exceeded, the stress in J zones was increased gradually until yield strength was reached, as shown in AB segments (bolt shank elastic transferring force stage) in **Figure 9A**. As the load was increased, the stress in J zones was increased to its tensile strength, as presented in BC segments (bolt shank plastic transferring force stage) in **Figure 9A**. Then, the stress in J zones was maintained constant at tensile strength until specimens failed, as presented in CD segments (failure stage) in **Figure 9A**.

4.1 Stress Analysis for the Force Transmission Mechanism of High-Strength Friction-Grip Bolts Under Bolts Shear off Failure

Figure 11 shows the changes in the Mises stress of HSFGBs and the maximum principal stress of concrete slabs in specimen SFRC-22-α1-8.8 during the whole loading process. For specimen SFRC-22-α1-8.8, at the beginning of loading, due to the pretension applied to HSFGBs, the Mises stress of HSFGBs was uniformly distributed along the bolt with an approximate value of about 350 MPa (**Figure 11A**) which was lower than its yield strength, while the concrete slabs around the bolts were compressed with 2.5 MPa stress (**Figure 11B**). Meanwhile, little relative slip between steel and concrete plates occurred, as described in the OA parts of the curves in **Figure 10**. When load value exceeded pretension-generated friction or reached

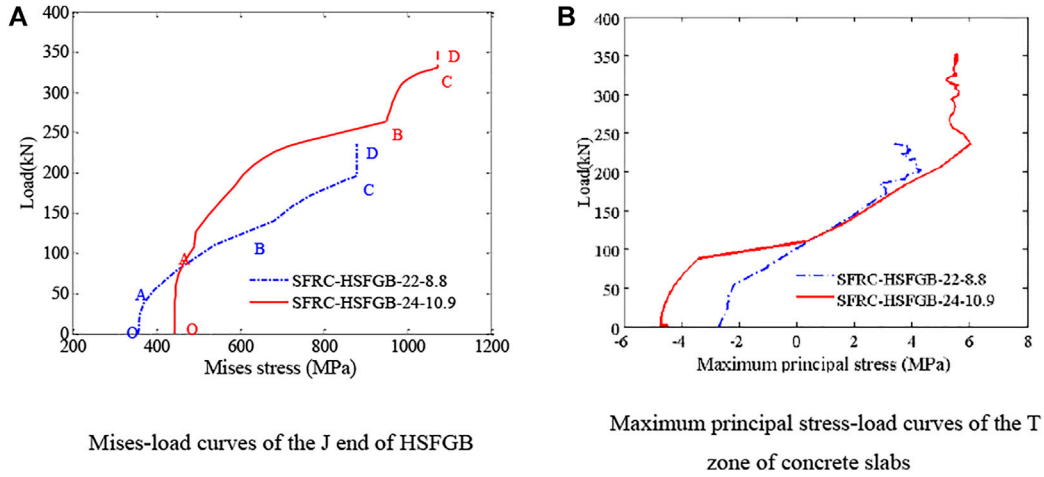

Mises-load curves of the J end of HSFGB

Maximum principal stress-load curves of the T zone of concrete slabs

FIGURE 9 | The stress-load curves of HSFGBs and concrete slabs in specimens.

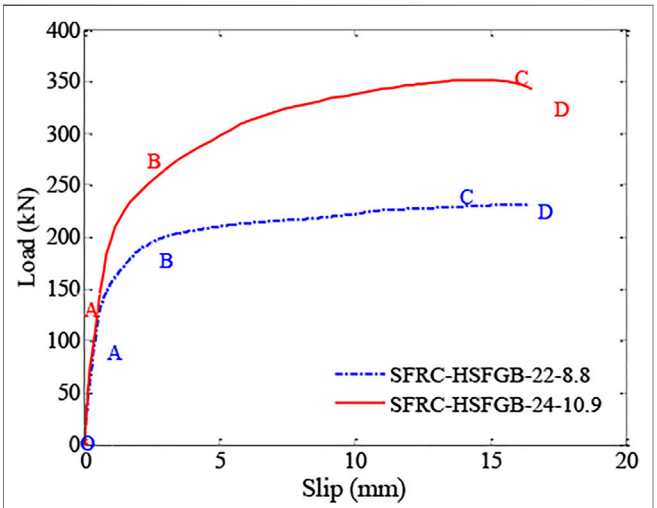

FIGURE 10 | The load-slip curves of HSFGBs in different specimens.

initial slip V_0 force, the serviceability limit state ended. As the load was increased to140 kN (about $0.6V_U$), HSFGB stress was unevenly distributed along the bolts and gradually decreased from J end to Q end (**Figure 11B**). HSFGB stress at the J end was about 620 MPa, which was close to yield strength. The maximum principal stress of concrete slabs was 2.10 MPa, which was lower than tensile strength. Hence, HSFGB yield was considered as the end of bolt shank elastic transferring force stage in these specimens. And relative slippage was linearly increased with the increase of load (**Figure 10** AB segments). Then, HSFGB stress at the J end was increased by increasing the load from 140 kN (about $0.6V_u$) to 240.5 kN (about V_u). HSFGB deformation was limited due to the constraints of surrounding steel plates and concrete slabs and stress at the J end quickly reached the tensile strength of 840 MPa (**Figure 11C**). However, the relative slip was increased with the increase of load and the relative slip growth rate was greater than the load growth rate, as described in the BC parts of the curves in the **Figure 10**. Then, relative slip continued to increase and the load was slightly decreased (**Figure 10** CD segments) until HSFGBs were sheared off at the interface of steel plates and concrete slabs.

4.2 Stress Analysis of the Force Transmission Mechanism of High-Strength Friction-Grip Bolts Under Concrete Splitting Failure

At the serviceability limit state, Mises stress in HSFGBs was uniformly distributed along the bolts in the SFRC-24-α1-10.9 specimen, which was similar to that of the SFRC-22-α1-8.8 specimen. Also, little relative slip between steel and concrete plates occurred (**Figure 10** OA segments). However, for the SFRC-24-α1-10.9 specimen, by the increase of load to 240 kN (about $0.7V_u$), HSFGB stress was unevenly distributed along the bolts and gradually decreased from J end to Q end (**Figure 12A**). HSFGB stress at J end was about 745 MPa which was lower than yield strength. Concrete slab stress was 5.46 MPa (**Figure 12B**), which was close to tensile strength. And the relative slip grew gradually and linearly. Therefore, the formation of concrete cracks was considered as the end of the bolt shank elastic transferring force stage for this specimen. HSFGB stress at the J end was increased by increasing load from 240 kN (about $0.7V_u$) to 365 kN (about V_u), and stress in concrete slabs reached tensile strength, resulting in concrete splitting failure while HSFGB maximum stress was about 1122 MPa, indicating that HSFGBs were under bending and shearing deformation, but not sheared off.

In summary, the force transfer process of HSFGBs in steel-SFRC push-out specimens was as follows: 1) friction transferring force stage or serviceability limit state: when the load was lower than V_0, load transferred by interface friction due to pretension and HSFGB stress was uniformly distributed along the bolts, while concrete slabs around the bolts were compressive with small slip between steel plates and concrete slabs. When load

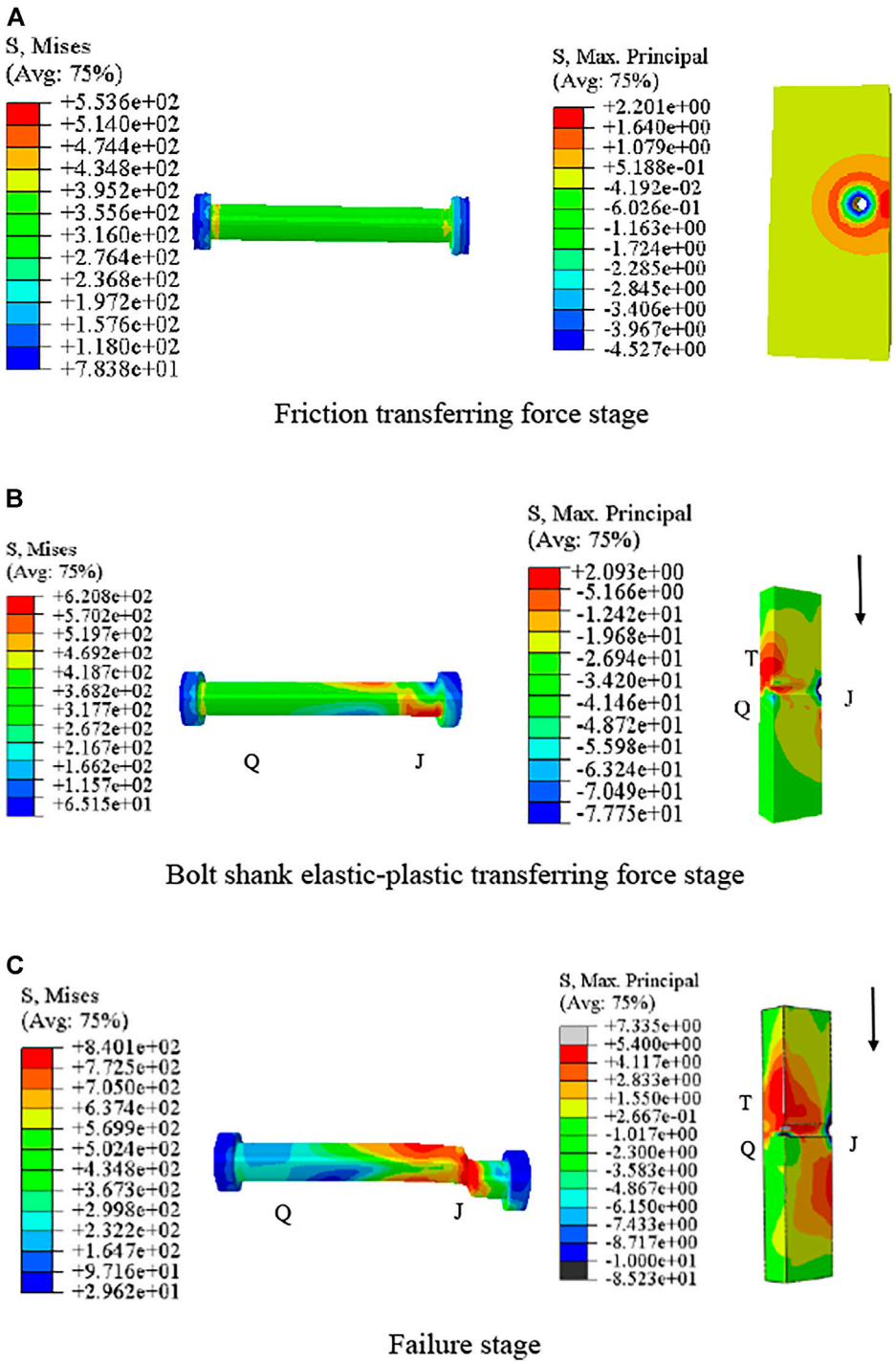

FIGURE 11 | Stress distribution in HSFGBs and concrete slabs in SFRC-22-α1-8.8 specimen(MPa).

reached initial slip force V_0, the end of serviceability limit state was reached. 2) Bolt shank elastic transferring force stage: when load was increased to 0.6–0.7V_u, HSFGB stress was unevenly distributed along the bolts and tensile stress was also increased in concrete slabs. HSFGB yield or concrete crack were regarded as the end of bolt shank elastic transferring force stage. 3) Bolt shank plastic transferring force stage: HSFGB stress was quickly increased to tensile strength and concrete stress was continuously increased as the load was increased from 0.6–0.7 V_u to V_u. 4) Failure stage: concrete crushing-splitting and bolt bending failures were more evident specimens when the diameter of HSFGB was large or tensile strength was high.

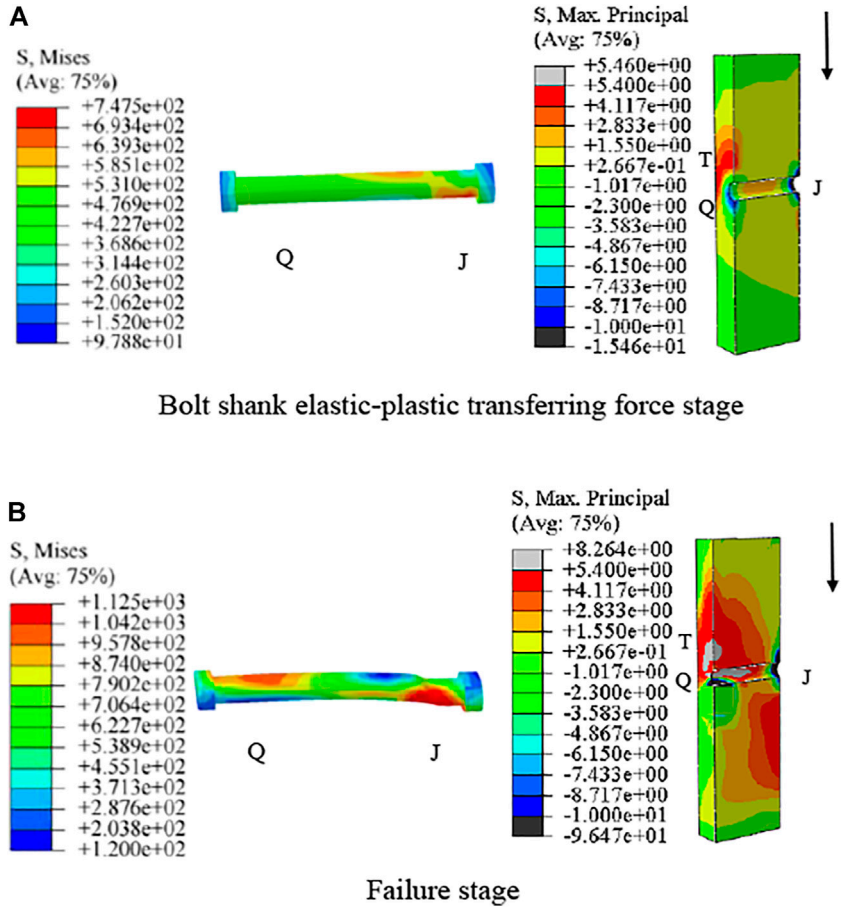

FIGURE 12 | Stress distribution in HSFGBs and concrete slabs in SFRC-24-α1-10.9 specimen (MPa).

Otherwise, bolt stress reached tensile strength resulting in shear fracture failure of the bolt.

5 THE SENSITIVITY DEGREES OF FACTORS ON THE SHEAR PERFORMANCE OF HIGH-STRENGTH FRICTION-GRIP BOLTS

5.1 Parameters

The previous results obtained by Zhang et al. (2020) showed that the main four factors affecting the HSFGB shear performance included concrete compressive strength (A), bolt diameter (B), tensile strength (C), and pretension (D). Due to several influencing factors and limited test conditions, it was difficult to conduct comprehensive tests. Therefore, the orthogonal statistics method was adopted to analyze the sensitivity of each influencing factor in HSFGB shear performance.

Generally, the diameters of HSFGBs applied in railway bridges and large factories are 20 and even 27 mm. Therefore, HSFGBs with diameters 20, 22, 24, and 27 mm were adopted to evaluate the influence of diameter on HSFGB shear performance. Grade 8.8 and 10.9 HSFGBs with tensile strengths of not less than 830 MPa are recommended to be applied in civil engineering. Different degrees of bolt pretension, i.e., 0.4, 0.6, 0.8, and 1, were adopted to investigate the influence of pretension on HSFGB shear performance. Concrete strength generally varies in the range of 40–70 MPa, which is commonly applied in steel-concrete composite structures. Therefore, four dimensions of each factor L_{16} (4^4) were adopted in orthogonal design, as listed in **Table 1**.

5.2 Analysis of Numerical Results

The numerical results obtained for each group are summarized in **Table 2**. For example, A1B1C1D1 represents the compressive strength of the concrete slab in this sample is 40MPa, while the diameter, tensile strength, and degrees of pretension of HSFGB are 20 mm, 830 MPa, and 0.4, respectively.

The total evaluation index was used for analysis by statistical method to investigate the influence of each parameter on the shear behavior of HSFGBs. w_i is the average value of numerical results obtained at the dimension i of the factors in any column, which was used to intuitively determine the degree of influence of each factor on the performance of HSFGBs as shown in **Figures 13–16** .The analysis of variance was performed by

TABLE 1 | Four factors and four dimensions of orthogonal design.

Four dimensions	Four factors			
	Concrete compressive strength (A) (MPa)	Bolt diameter (B) (mm)	Bolt tensile strength (C) (MPa)	Degrees of bolt pretension (D)
1	40	20	830	0.4
2	50	22	1000	0.6
3	60	24	1100	0.8
4	70	27	1200	1.0

TABLE 2 | The summary of numerical samples and results.

No	Sample name	Concrete compressive strength (MPa)	Bolt diameter (mm)	Bolt tensile strength (MPa)	Degrees of bolt pretension	V_0 (kN)	K_0 (kN/mm)	K_s (kN/mm)	V_u (kN)
1	A1B1C1D1	40	20	830	0.4	21.7	224.76	102.72	191.1
2	A1B2C2D2	40	22	1000	0.6	45.1	445.81	145.78	207.9
3	A1B3C3D3	40	24	1100	0.8	73.6	751.46	146.51	262.1
4	A1B4C4D4	40	27	1200	1	102.2	978.56	235.22	303.1
5	A2B1C2D3	50	20	1000	0.8	55.6	576.68	160.03	221.3
6	A2B2C1D4	50	22	830	1	70.5	700.36	187.02	269.4
7	A2B3C4D1	50	24	1200	0.4	42.3	438.74	157.48	330.8
8	A2B4C3D2	50	27	1100	0.6	66.9	684.47	233.21	349.5
9	A3B1C3D4	60	20	1100	1	74.5	737.76	168.94	247.2
10	A3B2C4D3	60	22	1200	0.8	62.5	631.54	205.71	319.9
11	A3B3C1D2	60	24	830	0.6	50.3	478.78	176.11	273.8
12	A3B4C2D1	60	27	1000	0.4	46.4	456.95	206.24	357.4
13	A4B1C4D2	70	20	1200	0.6	42.5	423.26	157.05	310.0
14	A4B2C4D1	70	22	1100	0.4	30.4	291.18	155.82	282.7
15	A4B3C4D4	70	24	1000	1	92.5	931.02	252.02	323.4
16	A4B4C4D3	70	27	830	0.8	78.2	788.76	220.33	320.2

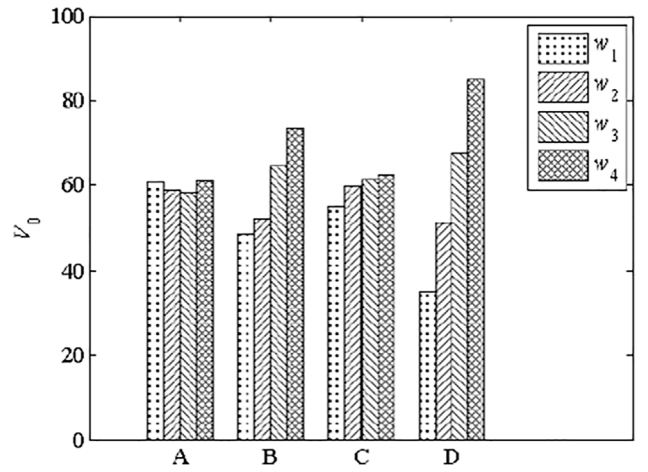

FIGURE 13 | Influence of the four factors on the initial slip force of HSFGBs.

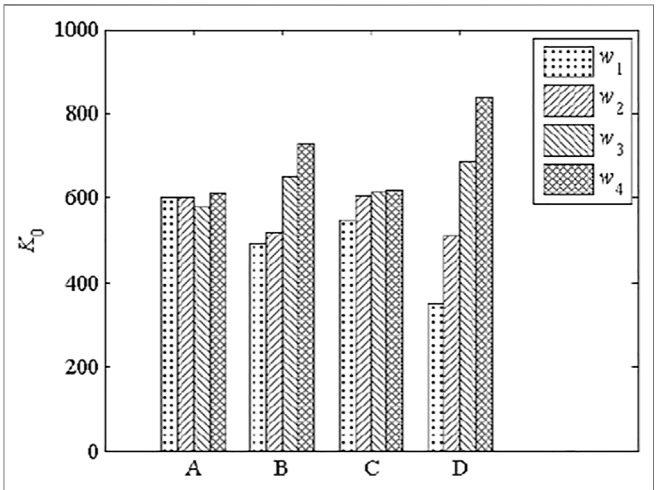

FIGURE 14 | Influence of the four factors on initial shear stiffness.

statistical software and the results are listed in **Tables 3–6**, where R is the range value of numerical results, while the values of χ and χ_a show the significance of factors' influence on the results.

5.2.1 The Sensitivity Degree of Each Factor to Force at Initial Slip of High-Strength Friction-Grip Bolts

Figure 13 shows that the average force at initial slip was increased with the increase of the diameter **(B)**, tensile strength **(C)**, and pretension degree **(D)** of HSFGBs, but was not significantly affected by concrete strength.

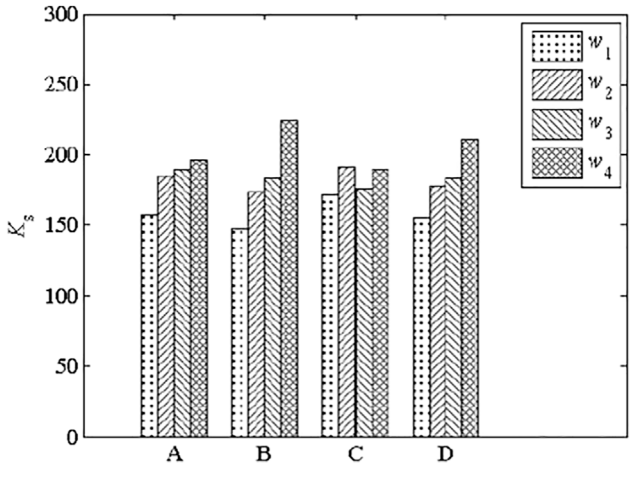

FIGURE 15 | Influence of the four factors on the post-slip stiffness of HSFGBs.

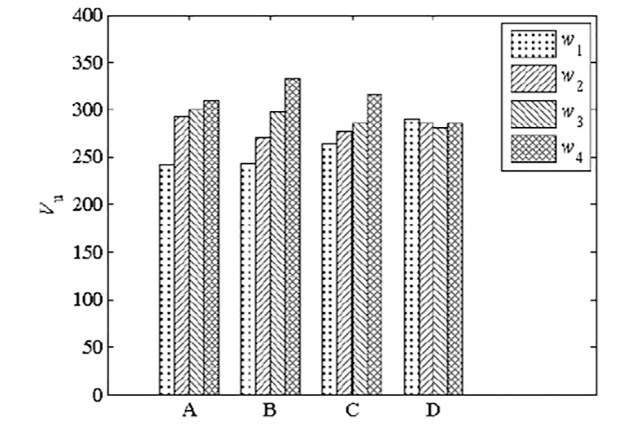

FIGURE 16 | Influence of the four factors on the ultimate capacity of HSFGBs.

Table 3 lists the range and variance analysis results of the initial slip force of HSFGBs. The ranges of pretension degree, diameter, and tensile strength of HSFGBs were 49.73, 24.86, and 7.21, respectively, while the χ values of the aforementioned three factors were all greater than the corresponding critical value χ_a, indicating that the influences of these three factors on initial slip force was more significant. However, the concrete strength range was 2.48 and the χ value of concrete strength was less than its critical value χ_a, indicating that concrete strength had little effect on initial slip force. According to the range analyses of results, the order of each factor affecting initial slip force was pretension degree (D)> bolt diameter (B)> its tensile strength (C)> concrete strength (A).

TABLE 4 | Results of range and variance analyses of initial shear stiffness.

Factor	Range (R)	Variance	χ	Critical value χ_a
Concrete strength (A)	32.31	774.668	0.64	$\chi_{0.1}$ = 3.289
Bolt diameter (B)	236.57	49916.33	50.14	
Bolt tensile strength (C)	69.86	4300.833	4.32	
Pretension degree (D)	484.02	177559.5	178.36	

TABLE 5 | Range and variance analysis results of the post-slip stiffness of HSFGBs.

Factor	Range (R)	Variance	χ	Critical value χ_a
Concrete strength (A)	38.75	1510.59	3.328	$\chi_{0.1}$ = 3.289
Bolt diameter (B)	76.56	4035.21	8.89	
Bolt tensile strength (C)	19.47	362.92	0.14	
Pretension degree (D)	55.23	2059.89	4.538	

TABLE 6 | Range and variance analysis results of the ultimate capacity of HSFGBs.

Factor	Range (R)	Variance	χ	Critical value χ_a
Concrete strength (A)	68.06	3714.333	8.29	$\chi_{0.1}$ = 3.289
Bolt diameter (B)	90.11	5935.667	13.247	
Bolt tensile strength (C)	52.31	1957.75	4.369	
Pretension degree (D)	9.65	62.208	0.075	

5.2.2 The Sensitivity Degree of Each Factor to Initial Shear Stiffness

Figure 14 shows that average initial shear stiffness was increased by increasing bolt diameter **(B)**, tensile strength **(C),** and pretension degree **(D)** but was not significantly affected by concrete strength.

Table 4 summarizes the results of range and variance analyses of initial shear stiffness. The ranges of bolt pretension degree, diameter, and tensile strength were 484.02, 236.57, and 69.86, respectively, while the χ values of the above three factors were all greater than their corresponding critical value χ_a, indicating that the influences of these three factors on initial shear stiffness were more significant. However, the range of concrete strength was 32.31 and its χ values were less than critical value χ_a, indicating that concrete strength had little effect on initial shear stiffness. According to the range analysis of initial shear stiffness results,

TABLE 3 | Range and variance analysis results of the initial slip force of HSFGBs.

Factor	Range (R)	Variance	χ	Critical value χ_a
Concrete strength (A)	2.48	6.256	1.292	$\chi_{0.1}$ = 3.289
Bolt diameter (B)	24.86	526.223	94.879	
Bolt tensile strength (C)	7.21	40.61	7.322	
Pretension degree (D)	49.73	1826.5	329.323	

the sensitivity degree of each factor to initial shear stiffness was as follows: pretension degree (D)> bolt diameter (B)> bolt tensile strength (C)> concrete strength (A).

5.2.3 The Sensitivity Degree of Each Factor to Post-slip Stiffness of High-Strength Friction-Grip Bolts

Figure 15 shows that post-slip stiffness was increased by increasing the bolt diameter **(B)**, pretension degree **(D)**, and concrete strength **(A)**, but was not significantly affected by tensile strength **(C)**. **Table 5** summarizes the results of range and variance analyses of post-slip stiffness. The ranges HSFGB pretension degree and diameter, as well as concrete strength, were 55.23, 76.56, and 38.75, respectively, while the χ values of the above three factors were all greater than their corresponding critical value χ_a, indicating that the influences of these three factors on post-slip stiffness were significant. However, the range of HSFGB tensile strength was 19.47 and its χ value was lower than the critical value χ_a, indicating that the tensile strength of HSFGBs had little effect on their post-slip stiffness. According to the range analysis of post-slip stiffness results, the sensitivity degree of each factor to post-slip stiffness was as follows: bolt diameter (B) > pretension degree (D)> concrete strength (A) > bolt tensile strength (C).

5.2.4 The Sensitivity Degree of Each Factor to the Ultimate Capacity of High-Strength Friction-Grip Bolts

Figure 16 shows that ultimate capacity was increased by increasing bolt diameter (B) and tensile strength (C) as well as concrete strength (A), but was not significantly affected by pretension degree (D). **Table 6** lists the results of range and variance analyses of ultimate capacity. The ranges of bolt tensile strength and diameter as well as concrete strength were 52.31, 90.11, and 68.06, respectively, while the χ values of the aforementioned three factors were all greater than their corresponding critical value χ_a, indicating that the influences of these three factors on ultimate capacity were significant. However, the range of HSFGB pretension degree was 9.65 and the χ value of pretension degree was less than its critical value χ_a, indicating that HSFGB pretension degree had little effect on ultimate shear strength. According to range analyses on ultimate capacity results, the influence degree of each factor on ultimate capacity was as follows: bolt diameter (B) > concrete strength **(A)** > bolt tensile strength (C) > bolt pretension degree (D).

Consequently, the sensitivity degree to each of these factors affecting the shear performance of HSFGBs was different. In general, pretension degree was the main factor affecting the shear performance of HSFGBs at serviceability limit states, while HSFGB diameter was the most important factor affecting stiffness and ultimate shear strength at ultimate limit state. From this perspective, it was important to control pretension loss through the application of double nuts and spring tightening. Additionally, HSFGBs with large diameter and high strength grade could improve the initial slip force, initial shear stiffness, and ultimate capacity of HSFGBs.

6 CONCLUSION

An accurate and reliable 3D finite element model has been developed to investigate the shear force transmission mechanism of HSFGBs in steel-SFRC composite beams. The following main conclusions were drawn.

1) Compared with the shear behavior of headed studs, the initial slip force of HSFGBs was more obvious due to the existing pretension of HSFGBs. At ultimate limit state, the ultimate capacities of headed studs and HSFGBs were approximate.
2) According to numerical results, the force transfer process of HSFGB steel-steel fiber reinforced concrete push-out specimens occurred as follows: 1) Friction transferring force stage or serviceability limit state: load reached to initial slip force V_0 which indicated the end of serviceability limit state. 2) Bolt shank elastic transferring force stage: HSFGB yield or concrete crack were regarded as the end of bolt shank elastic transferring force stage. 3) Bolt shank plastic transferring force stage: HSFGB stress was quickly increased to its tensile strength and concrete stress was continuously increased as load was increased from (0.6–0.7) V_u to V_u. 4) Failure stage: concrete crushing-splitting and bolt bending failures were more evident in specimens when HSFGB diameter was large or tensile strength was high. Otherwise, bolts were sheared off while bolt stress reached its tensile strength.
3) The sensitivity degree analysis results of the factors affecting the shear performance of HSFGBs revealed that pretension degree was the main factor affecting the shear performance of HSFGBs at the serviceability limit state, while HSFGB diameter was the most important factor affecting stiffness and ultimate shear strength at ultimate limit state. Therefore, considering the influences of various factors on HSFGB shear performance, HSFGBs with large diameter and high strength grade were recommended to be adopted in engineering, which could be installed by using double nuts or spring tightening to control the pretension loss of HSFGBs. Furthermore, selecting suitable concrete slabs to improve HSFGB shear performance was also very important.

DATA AVAILABILITY STATEMENT

The original contributions presented in the study are included in the article/Supplementary Material, further inquiries can be directed to the corresponding authors.

AUTHOR CONTRIBUTIONS

YjZ: data curation, finite element analysis, investigation, methodology, validation, and writing-original draft. JZ: software, funding acquisition, project administration, writing-review and editing. BC: finite element analysis, validation, and writing-original draft. YmZ: finite element analysis, writing-review and editing.

FUNDING

The research presented was funded by the National Natural Science Foundation of China (No. 52178280).

REFERENCES

Abas, F. M., Gilbert, R. I., Foster, S. J., and Bradford, M. A. (2013). Strength and Serviceability of Continuous Composite Slabs with Deep Trapezoidal Steel Decking and Steel Fibre Reinforced concrete. *Eng. Structures* 49, 866–875. doi:10.1016/j.engstruct.2012.12.043

Ataei, A., Zeynalian, M., and Yazdi, Y. (2019). Cyclic Behaviour of Bolted Shear Connectors in Steel-concrete Composite Beams. *Eng. Structures* 198, 109455. doi:10.1016/j.engstruct.2019.109455

Ban, H., Uy, B., Pathirana, S. W., Henderson, I., Mirza, O., and Zhu, X. (2015). Time-dependent Behaviour of Composite Beams with Blind Bolts under Sustained Loads. *J. Constructional Steel Res.* 112 (9), 196–207. doi:10.1016/j.jcsr.2015.05.004

British Standards Institution (2006). *Eurocode 4: Design of Composite Steel and concrete Structures: Part 1. 1 General Rules and Rules for Buildings, BS EN 1994-1-1*. London: BSI.

Brozzetti, J. (2000). Design Development of Steel-concrete Composite Bridges in France. *J. Constructional Steel Res.* 55, 229–243. doi:10.1016/s0143-974x(99)00087-5

Dallam, L. N., and Harpster, J. L. (1968). *Composite Beams Tests with HSFGB Shear Connectors*. Columbia, MO: Report for Missouri State Highway Department, Department of Civil Engineering, University of Missouri-Columbia.

Dallam, L. N. (1968). HSFGB Shear Connectors-Push Out Tests. *ACI J.* 65 (9), 767–769.

Dedic, D. J., and Klaiber, F. W. (1986). HSFGB as Shear Connectors in Rehabilitation Work. *Concrete Int.* 6 (7), 61–66.

Fang, Z. C., Jiang, H. B., Chen, G. F., Dong, X. T., and Shao, T. F. (2020). Behavior of Grouped Stud Shear Connectors between Precast High-Strength concrete Slabs and Steel Beams. *Steel Compos. Struct.* 34 (6), 837–854. doi:10.12989/scs.2020.34.6.837

Fang, Z., Fang, H., Huang, J., Jiang, H., and Chen, G. (2022). Static Behavior of Grouped Stud Shear Connectors in Steel-Precast UHPC Composite Structures Containing Thin Full-Depth Slabs. *Eng. Structures* 252, 113484. doi:10.1016/j.engstruct.2021.113484

Fang, Z., Liang, W., Fang, H., Jiang, H., and Wang, S. (2021). Experimental Investigation on Shear Behavior of High-Strength Friction-Grip Bolt Shear Connectors in Steel-Precast UHPC Composite Structures Subjected to Static Loading. *Eng. Structures* 244, 112777. doi:10.1016/j.engstruct.2021.112777

Gao, D. Y. (1991a). Stress-strain Curves of Steel Flber Reinforced concrete under Axial Compression. *J. Hydraulic Eng.* 10, 63–68.

Gao, D. Y. (1991b). Stress-strain Curves of Steel Flber Reinforced concrete under Axial Tension. *J. Water Power* 11, 56–58.

GB/T 3632-2008 (2008). *National Standards of the People's Republic of China. Sets of Torshear Type HSFGB Hexagon Nut and plain Washer for Steel Structure*. Beijing: Standards Press of China.

Han, Q., Wang, Y., Xu, J., and Xing, Y. (2015). Static Behavior of Stud Shear Connectors in Elastic concrete-steel Composite Beams. *J. Constructional Steel Res.* 113, 115–126. doi:10.1016/j.jcsr.2015.06.006

Johnson, R. P. (2006). *Composite Structures of Steel and Concrete: Beams, Slabs, Columns, and Frames for Buildings*. Oxford, United Kingdom: Blackwell Publishing.

Khaloo, A. R., and Afshari, M. (2005). Flexural Behaviour of Small Steel Fiber Reinforced concrete Slabs. *Cement Concrete Comp.* 27 (1), 161–169. doi:10.1016/j.cemconcomp.2004.03.004

Kwon, G., Engelhardt, M. D., and Klinger, R. E. (2010). Behaviour of post-installed Shear Connectors under Static and Fatigue Loading. *J. Constr Steel Res.* 66 (6), 532–561. doi:10.1016/j.jcsr.2009.09.012

Kwon, G., Engelhardt, M. D., and Klingner, R. E. (2011). Experimental Behavior of Bridge Beams Retrofitted with Postinstalled Shear Connectors. *J. Bridge Eng.* 16 (4), 536–545. doi:10.1061/(asce)be.1943-5592.0000184

Lin, W., Yoda, T., and Taniguchi, N. (2016). Application of SFRC in Steel-concrete Composite Beams Subjected to Hogging Moment. *J. Constr Steel Res.* 101, 175–183. doi:10.1016/j.jcsr.2014.05.008

Liu, X., and Bradford, M. A. (2016). Finite Element Modelling of Steel–concrete Composite Beams with High-Strength Friction-Grip Bolt Shear Connectors. *Finite Elem. Anal. Des.* 108, 56–65. doi:10.1016/j.finel.2015.09.004

Liu, X., Bradford, M. A., and Lee, M. (2015). Behaviour of High-Strength Friction-Grip Bolted Shear Connectors in Sustainable Composite Beams. *J. Struct. Eng. ASCE* 161 (6), 1–12. doi:10.1061/%28ASCE%29ST.1943-541X.0001090

Lius, I., Bradford, M. A., Uy, B., Filonov, A., and Vrcelj, Z. (2006). "Shear Connection in Composite Secondary Beams with Trapezoidal Profiled Fibre Reinforced concrete Slabs, Nineteenth Australasian Conference on the Mechanics of Structures and Materials," in 19th Australasian Conference on the Mechanics of Structures and Materials, Christchurch, New Zealand, 95–101.

Nakamura, S.-i., Momiyama, Y., Hosaka, T., and Homma, K. (2002). New Technologies of Steel/concrete Composite Bridges. *J. Constructional Steel Res.* 58 (1), 99–130. doi:10.1016/s0143-974x(01)00030-x

Oehlers, D. J., and Bradford, M. A. (1995). *Composite Steel and Concrete Structural Members: Fundamental Behaviour*. Oxford, United Kingdom: Pergamon Press.

Pavlović, M., Marković, Z., Veljković, M., and Buđevac, D. (2013). Bolted Shear Connectors vs Headed Studs Behaviour in Push-Out Tests. *J. Constr Steel Res.* 88, 136–169. doi:10.1016/j.jcsr.2013.05.003

Taniguchi, N., Ikeda, M., Ikariyama, H., and Irube, T. (2007). "Experimental Study on a Crack Formation for Railway Composite Girders With Negative Bending," in Proceedings of the Third International Conference on Steel and Composite Structures ICSCS07, Manchester, 915–920.

Wang, S. D., Fang, Z. C., and Chen, G. F. (2021). Numerical Analysis on Shear Behavior of Grouped Head Stud Shear Connectors between Steel Girders and Precast concrete Slabs with High-Strength concrete-filled Shear Pockets. *J. Bridge Eng. ASCE* 26 (6), 04021030. doi:10.1061/(asce)be.1943-5592.0001727

Zhang, Y. J., Chen, B. C., Liu, A. R., Pi, Y. L., Zhang, J. P., Wang, Y., et al. (2019). Experimental Study on Shear Behaviour of HSFGBconnection in Prefabricated Steel-concrete Composite Beam. *Compos. Part. B-eng.* 159, 681–689. doi:10.1016/j.compositesb.2018.10.007

Zhang, Y., Liu, A., Chen, B., Zhang, J., Pi, Y.-L., and Bradford, M. A. (2020). Experimental and Numerical Study of Shear Connection in Composite Beams of Steel and Steel-Fibre Reinforced concrete. *Eng. Structures* 215, 110707. doi:10.1016/j.engstruct.2020.110707

Conflict of Interest: The authors declare that the research was conducted in the absence of any commercial or financial relationships that could be construed as a potential conflict of interest.